MEASUREMENT OF DEVELOPING TURBULENT FLOWS IN A ROTATING 90 DEGREE BEND WITH SQUARE CROSS-SECTION

Young Don Choi
Department of Mechanical Engineering, Korea University
Sungpukku, Seoul, 136-701, Korea. Tel: 82-2-3290-3355
ydchoi@korea.ac.kr

Kun Ho Chun
Department of Mechanical Engineering, Korea University
Sungpukku, Seoul, 136-701, Korea. Tel: 82-2-926-5908
khchun@korea.ac.kr

Dong Chul Kim
Department of Mechanical Engineering, Korea University
Sungpukku, Seoul, 136-701, Korea. Tel: 82-2-926-5908
dckim4296@hanmail.net

ABSTRACT
Mean velocity and Reynolds stress components of the developing turbulent flows in a rotating 90 degree bend with square cross-section were measured by a hot-wire anemometer. Effects of the centrifugal and Coriolis forces generated by the curvature and rotation of bend on the mean motion and turbulence structures are investigated experimentally. Results show that the Coriolis force associated with the rotation of the bend may act both through the mean motion and turbulent structures, thereby changing the pressure fields, mean and turbulent velocities distributions.

INTRODUCTION
Information on the turbulent flows in rotating bend are of great engineering importance, for instance, in the design of turbomachinery. In such flows, Coriolis and centrifugal forces associated with the curvature and rotation of bend may act both through the mean motion and turbulence structures. Consequently, the reacting forces on the mean motion may encounter rapid changes in direction and magnitude as the flow progresses along the passage. If the forces are added in a productive way, the resultant force may promote the generation of secondary flow while the forces are combined in a destructive way, it may decrease the secondary flow. It is highly desirable to decouple the contributions of the reacting forces on the mean motion and turbulence structures. However, it is not easy to isolate their contributions in the rotating curved duct flows in practice.

There have been extensive studies on the effects of Coriolis and centrifugal forces on the rotating plane channel flows. They include the large eddy simulation of Kim[1983] and Tafti & Vanka[1991], the experimental study of Koyama and Ohuchi[1985], the direct numerical simulation of Kristofferson and Andersson[1990], and the application of second-moment closures of Launder et al.[1987], and Launder and Tselepidakis[1994].

However, only a little attention has been paid to the turbulent flows in the rotating bends. The turbulent flow in a rotating 90 degree bend with square cross-section has several qualities that make it well suited as a bench mark test flow for the development of second moment turbulence closure models. In this type of flows, the effects of Coriolis and centrifugal forces on the mean motion and turbulence structures can easily be decoupled due to its simple shape of the flow passage.

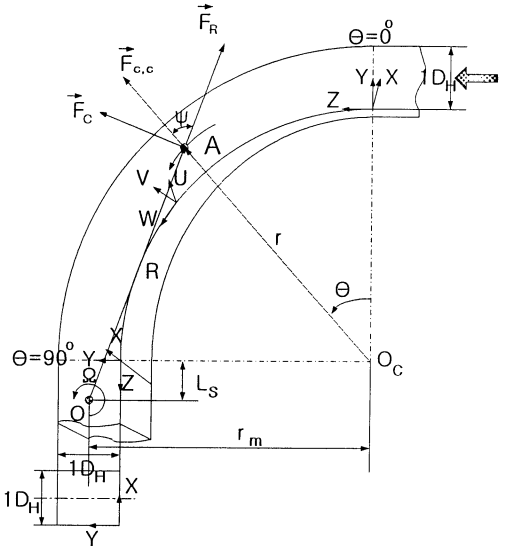

Figure 1: Schematic diagram showing the rotating bend and tangents, the two coordinates systems and the three velocity components

In the present study, the mean velocity and Reynolds stress components of the developing turbulent flows in a rotating 90 degree bend with square cross-section are measured by hot-wire anemometer with variation of Reynolds and rotation numbers. Pressure coefficients of the inner and outer walls are also measured by pressure transducer. Figure 1 shows the schematic diagram of a rotating 90 degree bend with square cross-section, and defines the coordinate system and symbols used. X and Y map the cross-sectional plane, while progress around the bend is expressed through the angle θ.

EXPERIMENT

Experimental Apparatus

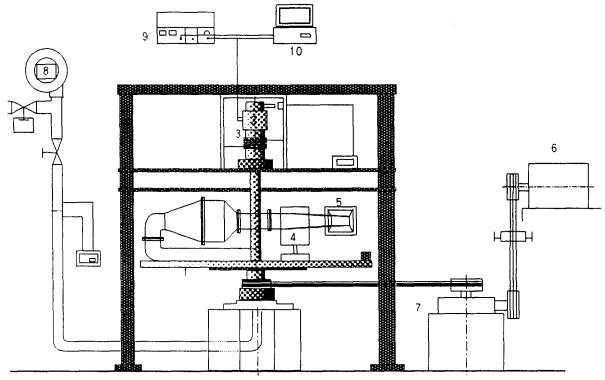

Figure 2: Schematic diagram of experimental apparatus

1 : Rotating disc
2 : Slip-ring for hot-wire anemometer and traversing mechanism
3 : Slip-ring for AC power
4 : Traversing mechanism
5 : Test section
6 : Variable motor
7 : Speed reducer
8 : Blower
9 : Hot-wire anemometer
10 : Personal computer

The schematic diagram of experimental apparatus and the plan view of the rotating disc are Figure2 and Figure 3. It is composed of a test section of 90 degree bend with square cross-section, rotating disc of 1.95m diameter, Ag-Ni precision slip ring constructed to transmit the signal from the rotating test section to the stationary anemometer, electric power supply for automatic traversing mechanism, variable speed motor, speed reduction gear mechanism, centrifugal blower, orifice flowmeter, and hot-wire anemometer system. The test section is constructed from 8mm thickness polyester sheet providing rigid transparent walls. Honeycomb and wire mesh are installed in front of the test section to

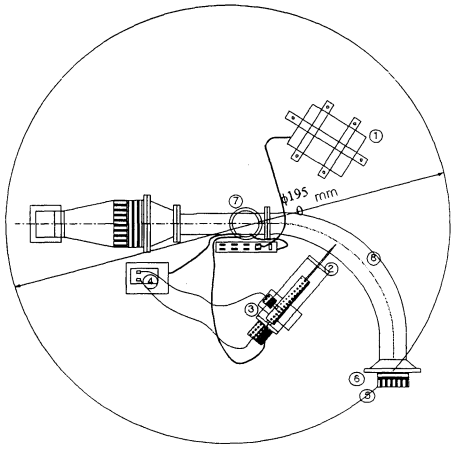

Figure.3: Plan view of rotating disc

1 : Controlling computer
2 : Rotating probe
3 : Automatic traversing mechanism
4 : Control box 5 : Setting chamber
6 : Turbulence generator 7 : Slip ring
8 : Test section

eliminate the secondary motion and turbulence involved in the intake flow. Just after the wire mesh, a turbulence generator made of 5mm diameter tube bank in 10.4mm pitch, is installed to generate uniform inlet turbulence. The speed of the rotating disc is controlled by a variable speed motor and a bevel gear speed reduction mechanism. The hot-wire probe is traversed by an automatic mechanism which is installed on the rotating disc. Translation tolerance of the automatic traversing mechanism is 1/200mm and the rotation tolerance is 1/2 deg. Air flow through the test section is provided by a centrifugal blower, and the flowrate is measured by a $D-1/2D$ orifice flowmeter.

Test section and experimental program

Two kinds of test sections were used for the present experiments. One is the test section A shown in Figure 4. Test section A is composed of 90 degree bend of square cross-section with 80mm hydraulic diameter. The lengths of inlet and outlet tangents of the bend are 1 and 2.325 hydraulic diameter. In the test section A, static pressure coefficients of inner and outer walls, and mean velocity components for the inward flow mode were measured with variation of rotation numbers. Experimental program for the test section A is shown in Table1. As shown in Figure 4, pressure holes are installed on the inner and outer walls along the symmetric plane of the bend at every 5 degree. Velocity holes are installed at the 7 stations, $-0.5D_H$, $-0.25D_H$, 0°, 22.5°, 45°, 67.5° and 90° on the outside wall. At each station, 4 velocity holes are located at the positions of $2X/D_H$=0.25, 0.5, 0.75, 1.0 of each station.

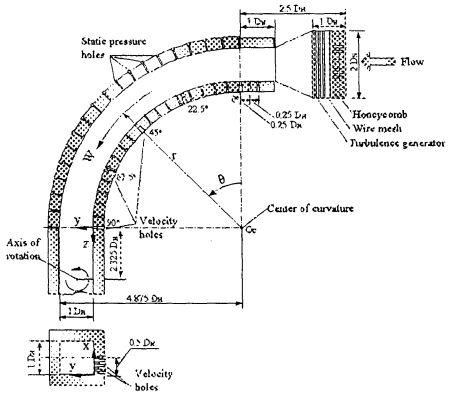

Figure 4 : Schematic diagram of test section A

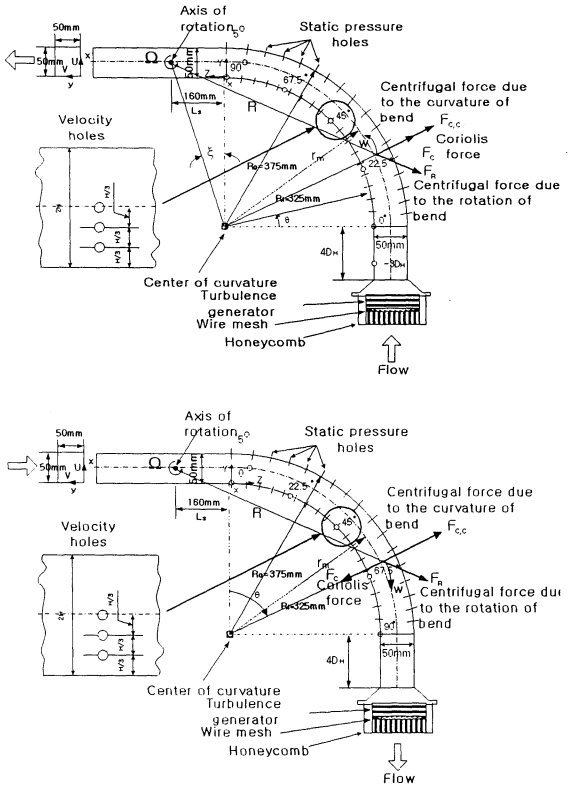

Figure 5: Schematic diagram of test section B

Test section B shown in Figure 5 is composed of 90 degree bend of square cross-section with 50mm hydraulic diameter. Velocity holes are installed at the 6 stations, $-3\,D_H$, 0°, 22.5°, 45°, 67.5°, 90°. Three velocity holes are located at the position of $2X/D_H$ =0.28, 0.64 and 1.0 of each station. In the test section B mean velocity and Reynolds stress components were measured for both the inward and outward flow modes with variation of rotation and Reynolds numbers. Table.2 shows the experimental program for the test section B.

Reynolds number	Rotating speed(rpm)	Rossby number	Rotation number	Dean number
20,000	0	0	0	9,562
40,000	0	0	0	19,124
40,000	45	0.048	0.210	19,124
40,000	60	0.064	0.280	19,124
20,000	60	0.128	0.561	9,562
20,000	60	-0.128	-0.561	9,562
20,000	75	-0.160	-0.701	9,562

Table 1 Experimental program for the test section A

Reynolds number	Rotation speed(rpm)	Rossby number	Rotation number	Dean number
17,000	0	0	0	6,425
8,500	0	0	0	3,213
17,000	20	0.03	0.21	6,425
8,500	20	0.06	0.42	3,213
17,000	20	-0.03	-0.06	6,425
8,500	20	-0.06	-0.42	3,213

Table 2 Experimental program for the test section B

The six orientation hot-wire technique was applied to measure the mean velocity and Reynolds stress components.

RESULTS AND DISCUSSIONS

Distributions of pressure coefficients on the inner and outer walls are compared in Figure 6 with

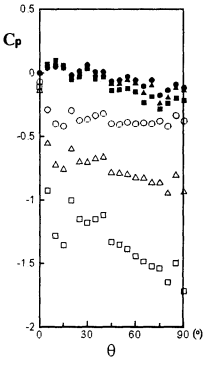

○: outer wall ●: inner wall for Rc = 0
△: outer wall ▲: inner wall for Rc = 0.210
□: outer wall ■: inner wall for Rc = 0.280

Figure 6 Comparison of measured pressure coefficients in the inward flow mode for Re=40,000

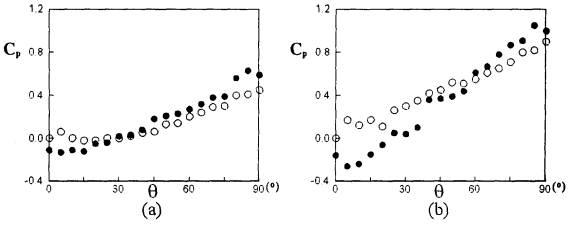

○ : outer wall ●: inner wall

Figure 7. Comparison of measured pressure coefficients in the outward flow mode for Re=20,000 and (a) Rc=-0.561, (b) Rc=-0.701

variation of rotation numbers. The pressure coefficient is defined as

$$C_P = \frac{P - P_r}{\frac{1}{2}\rho W_B^2} \quad (1)$$

where W_B is bulk mean velocity, P is local mean pressure and P_r is reference pressure. Outer wall pressure at the bend inlet was adopted for the reference pressure P_r. As the flow enters the bend, the pressure coefficient of the outer wall rises quickly while that of inner wall drops almost as quickly, but after the entrance region, both pressure coefficients drop again slowly. However, as increasing the rotation number of the bend, differences between the inner and outer wall pressure coefficients also increase. For the inward flow mode, Coriolis forces are added to the centrifugal forces associated with bend curvature in a productive way to the outward radial direction so that it may increase the difference of pressure coefficients between the inner and outer walls. Pressure coefficients of the inner wall appear to vary more sensitive with the increase of rotation number than those of the outer walls.

It is of interest in Figure 7 to compare the measured pressure coefficients for the outward flow mode in which rotation number has negative value. In the outward flow mode, the radial component of Coriolis force diminishes the centrifugal force associated with the bend curvature in a destructive way. Furthermore, in the entrance region of the bend, the Coriolis force exceeds the centrifugal force so that it make the pressure cofficients of inner wall larger than those of outer wall. But as the flow progresses around the bend, the trend is reversed. At Rc = -0.561, the reverse of pressure coefficients occurs near θ=30° while at Rc = -0.701 the reversal point moves to θ=55°.

Figure 8 shows the comparison of the longitudinal variation of measured mean streamwise and radial velocity profiles of the rotating and stationary bend flows for the inward flow mode. The solid symbol indicates the mean velocity components of the stationary bend flow while the open symbol does those of the rotating bend. As the flow progresses along the bend, the location of maximum mean streamwise velocity shifts toward outer wall both in the stationary and rotating bend flows. In this type of inward flow mode, the rotation of bend makes the Coriolis and the centrifugal forces be added in a productive way to radial outward direction to increase the secondary flow intensity, thereby promoting the shift of the location of maximum mean streamwise velocity toward the outer wall in the entrance region of the bend. However, in the rotating bend flow, the shifting of the location of maximum velocity stops after $\theta = 45^0$ into bend. Earlier break down of counter rotating vortex pair into a multi-cellular pattern which may be caused by the reaction of the centrifugal force due to rotation of bend, may prevent the further shift of the location of maximum mean streamwise velocity toward outer wall.

The decrease in the level of turbulence energy are found in Figure 9 near the suction side in the rotating bend flow. There is no Coriolis term in the turbulence energy equation. Launder and Tselepidakis[1994] applied second moment closure

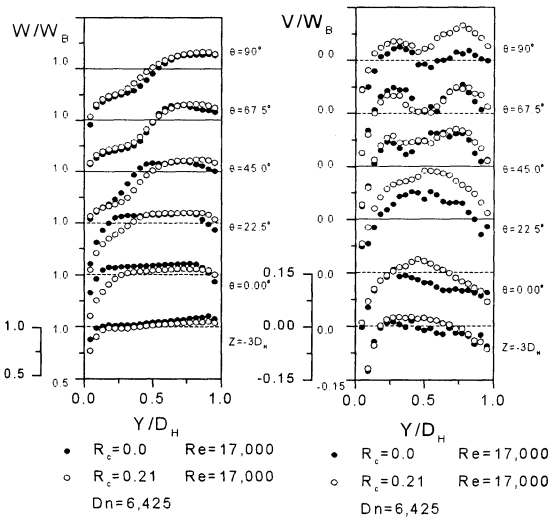

Figure 8 : Logitudinal variation of measured normalized mean streamwise velocity (W/W_B)and mean radial velocity (V/W_B) along the center symmetry plane for the inward flow mode.

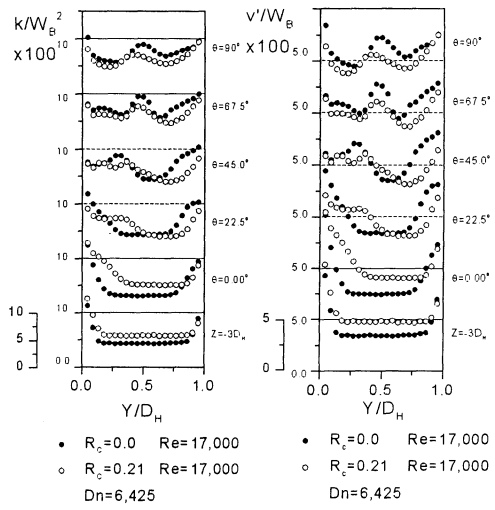

Figure 9 : Longitudinal variation of measured turbulence energy (k/W_B^2) and normalized rms radial turbulence velocity for the inward flow mode.

to the rotating plane channel flow and computationally validated the effects of Coriolis production term in $\overline{vw}$ equation on the level of turbulent energy. In the rotating straight channel flow the Coriolis production term $-2(\overline{w^2} - \overline{v^2})\Omega$ in the $\overline{vw}$ equation decreases the positive level of $\overline{vw}$

near the suction surface so that it results in the decrease of the level of turbulence energy and Reynolds normal stresses in that region while generating opposite effects near the pressure surface.

In Figure 9 we can clearly find the effects of Coriolis production term in $\overline{vw}$ equation on the level of turbulence energy in the inlet tangent and entrance region of rotating bend of square cross-section. However, as the flow progresses around the bend, the reduction of turbulence energy near the suction surface remains up to bend outlet while near the pressure surface the level of turbulence energy of the rotating bend fall bellow those of the stationary bend. In the inward flow mode, productive addition of Coriolis and centrifugal forces to the outward radial direction may increase the secondary flow intensity and advance the breakdown of counter rotating secondary flow vortex to multi-cellular pattern. The earlier break down of counter rotating vortex near the pressure surface may prevent the increase of turbulent energy in that region.

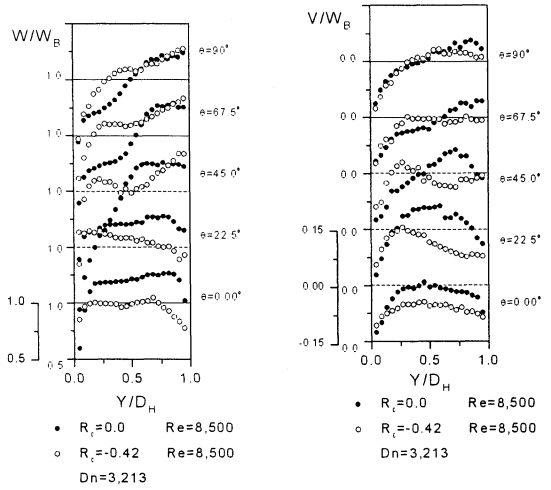

Figure 10 : Logitudinal variation of measured normalized mean streamwise velocity(W/W_B) and mean radial velocity(V/W_B) along the center symmetry plane for the outward flow mode.

In the outward flow mode, destructive addition of Coriolis force and centrifugal force due to bend curvature may decrease the secondary flow intensity. Figure. 10 shows the comparison of the measured mean streamwise and radial velocity profiles of the rotating and stationary bend flows for the outward flow mode. The rotation of bend make the mean streamwise velocity profiles be flatter and shift the location of the maximum velocity slowly toward outer wall. Much reduction of secondary flow intensity is found in the entrance region of the bend. However, at the bend exit, magnitude of normalized mean radial velocity of the rotating bend increase nearly up to the level of stationary bend.

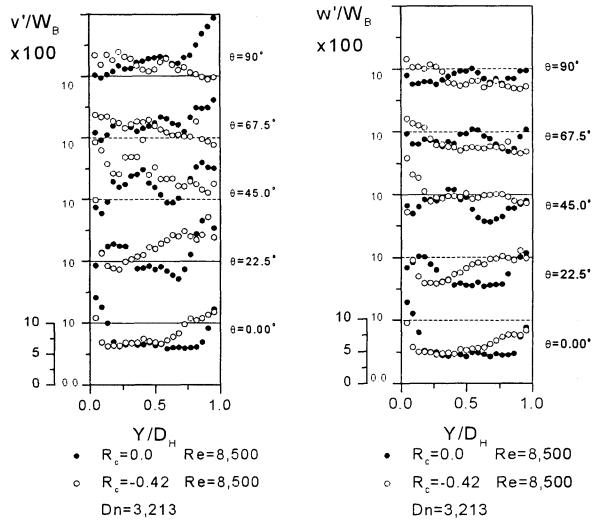

Figure 11 : Longitudinal variation of measured normalized rms streamwise turbulent velocity(w'/W_B^2) and radial turbulence velocity(v'/W_B) for the outward flow mode

Comparison of v'/W_B and w'/W_B in Figure 11 shows the more obvious evidence of the bend rotation on the levels of Reynolds stresses. Decrease of secondary flow intensity due to the destructive addition of Coriolis and centrifugal forces for outward flow mode makes the effect of Coriolis production term $-2\Omega(\overline{w^2}-\overline{v^2})$ in $\overline{vw}$ equation on the levels of turbulence energy and Reynolds normal stresses come into view. Opposite sign of the production rate terms, $\overline{vw}W/r$ and $4\Omega\overline{vw}$, in $\overline{v^2}$ and $\overline{w^2}$ equations may cause the different trends in the variations of $\overline{v^2}$ and $\overline{w^2}$ profiles near the suction surface. In the entrance region, the levels of v'/W_B near wall side are larger than those of core region. But after $\theta = 45°$ the level of v'/W_B of the core region becomes larger than those of near wall regions. This is due to the change of sign in the Coriolis production term $2\Omega_1(\overline{w^2}-\overline{v^2})$ in $\overline{vw}$ equation as with the increase of $\overline{v^2}$ over the $\overline{w^2}$ as shown in Figure 11.

Figure 12 compares the variations of measured streamwise velocity profiles of the rotating bend flows with those of the stationary bend for $R_C = 0.561$ and $D_H = 9{,}562$. As the flow enters the bend from the straight inlet tangent, it meets with the abrupt favorable pressure gradient in the inner wall side, on the other hand, the adverse pressure gradient in the outer wall side. This difference of pressure gradients in the inner and outer wall sides in the entrance region of bend may accelerate the flow in the inner wall side and decelerate the flow in the

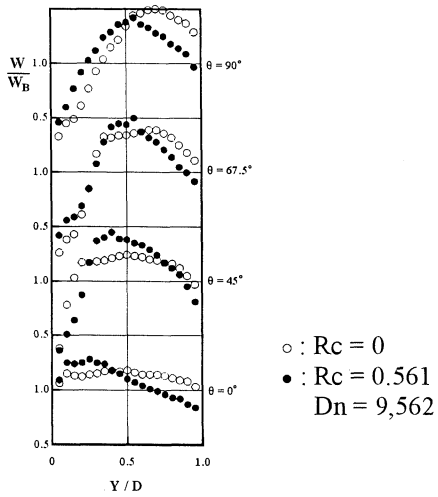

Figure 12 : Development of streamwise mean velocity profiles along the symmetry plane

outer wall side. However, as the flow progresses along the bend, the location of maximum mean streamwise velocity shifts toward the outer wall both in the stationary and rotating bend flows. However, for this the rotating bend flow of high rotation and dean numbers, the shift of maximum streamwise velocity stops moving near Y/D=0.5. In the stationary bend, the centrifugal force and radial pressure gradient imbalance may induce a pair of large counter-rotating Eckmann vortex and grows up to θ=90 degree. It is known that, after θ=90 degree, the Eckmann vortex pair breaks down and Dean vortices appears in the outer wall region. Lee [1992] found in the calculation of a rotating 90 degree bend flow with square cross-section that the rotation of bend may advance the appearance of a large Dean vortex pair up to θ=45 degree. This large Dean vortex pair appeared in the entrance region of the bend near outer wall surface may prevent the further shift of the maximum streamwise velocity toward the outer wall region and decrease the level of mean streamwise velocity of the outer wall region.

CONCLUSIONS

From the experimental investigations on the effects of the rotation of 90 degree bend with square cross-section on the mean motion and turbulence structures, the following conclusions are drawn.

1. Productive addition of Coriolis force and centrifugal force due to bend curvature to the outward radial direction increase the secondary flow intensity in the entrance region of the bend. However, after 45 degree of the bend, centrifugal force due to the rotation of bend may promote the break down of the counter rotating vortex pair into multi-cellular pattern, thereby decreasing the production rate of turbulence energy.

2. In the rotating 90 degree bend flows with square cross-section, Coriolis production term in $\overline{vw}$ equation may decrease both the Reynolds stresses and turbulent energy near the suction surface while remaining those of near pressure surface due to the advanced break down of counter-rotating vortex pair into multi-cellular pattern near pressure surface.

3. The effects of Coriolis production terms in $\overline{vw}$ equation on the level of turbulence energy come into view more clearly for the outward flow mode due to the decrease of secondary flow intensity according to the destructive addition of Coriolis and centrifugal forces.

References

Kim, J., 1983, "The effect of rotation on the turbulent structure", Proc. of 4th International Symposium on Turbulent Shear Flows, Karlsruhe, pp. 6-14.

King, C.F., 1978, Ph.D. Thesis, Univ. College of Wales, Cardiff, Wales.

Kristoffersen, R., Nilsen, P.J. and Andersson, 1990, "Validation of Reynolds stress closures for rotating channel flows by means of direct numerical simulations", Proc. International Symposium on Engineering Turbulence Modelling and Measurments, Dubrovinik, pp. 55-64.

Koyama, D.K. and Ohuchi, M., 1985, Proc. of 5th International Symposium of Turbulent Shear Flows, Cornell, pp. 21-19.

Launder, B.E., Tselepidalsis, D.P. and Younis, B.A., 1987, "A second-moment closure study of rotating channel flow", J. Fluid Mech., vol. 183, pp. 63-75.

Launder, B.E. and Tselepidalsis, D.P., 1994, "Application of a new second moment closure to turbulent channel flow rotating in orthogonal mode", International Journal of Heat and Fluid Flow, vol.15, no.1, pp. 2-10.

Tafti, D.K. and Vanka, S.P., 1991, "A numerical study of the effect of spanwise rotation on turbulent channel flow", Phys. Fluids A vol.3, no.4, pp. 642-656.